Endometrial stem cell-derived exosomes repair cisplatin-induced premature ovarian failure via Hippo/YAP pathway

Lijun Wang
xi'an jiaotong daxue diyi fushu yiyuan: Xi'an Jiaotong University Medical College First Affiliated Hospital
Lihui Wang
xi'an jiaotong daxue diyi fushu yiyuan: Xi'an Jiaotong University Medical College First Affiliated Hospital
Rongli Wang
xi'an jiaotong daxue diyi fushu yiyuan: Xi'an Jiaotong University Medical College First Affiliated Hospital
Ting Xu
xi'an jiaotong daxue diyi fushu yiyuan: Xi'an Jiaotong University Medical College First Affiliated Hospital
Jingyuan Wang
xi'an jiaotong daxue diyi fushu yiyuan: Xi'an Jiaotong University Medical College First Affiliated Hospital
Zhiwei Cui
xi'an jiaotong daxue diyi fushu yiyuan: Xi'an Jiaotong University Medical College First Affiliated Hospital
Feiyan Cheng
xi'an jiaotong daxue diyi fushu yiyuan: Xi'an Jiaotong University Medical College First Affiliated Hospital
Wei Wang
xi'an jiaotong daxue diyi fushu yiyuan: Xi'an Jiaotong University Medical College First Affiliated Hospital
Xinyuan Yang (✉ 1924484009@qq.com)
Xi'an Jiaotong University https://orcid.org/0000-0002-0703-7143

Research Article

Keywords: chemotherapy, endometrial stem cells, exosomes, Hippo, YAP.

Posted Date: May 25th, 2022

DOI: https://doi.org/10.21203/rs.3.rs-1656612/v1

Abstract

Background

Stem cells have been documented as a new therapeutic method for ovarian injuries such as premature ovarian failure (POF). However, effects of exosomes (Exos) derived from human endometrial stem cells (EnSCs) on diminished ovarian failure remain to be carefully elucidated. Therefore, our study aims to investigate the mechanisms of EnSC-Exos is related to Hippo signal pathway in the recovery of the cisplatin-induced granulosa cell injury model *in vitro* and the POF mice model *in vivo*.

Methods

Exosomes derived from human EnSCs were isolated by ultracentrifugation and identified by electron microscopy and western blot (WB) analysis, stained by PKH26, respectively. The mechanism involving suppression of Hippo signaling pathway and activation of Yes-associated protein (YAP) was investigated for evaluating EnSC-Exos therapeutic effects in the cisplatin-induced granulosa cell injury model *in vitro* using flow cytometry, WB, qRT-PCR, immunofluorescence and EdU staining. Hematoxylin-eosin staining, ELISA and immunohistochemistry analysis were used for evaluating EnSC-Exos therapeutic effects in POF mice model.

Results

We established successful construction of the cisplatin-induced granulosa cell injury model and evaluated Hippo signaling pathway activation in cisplatin-damaged granulosa cells (GCs). Furthermore, laser scanning confocal microscope and immunofluorescence demonstrated that EnSC-Exos can be transferred to cisplatin-damaged GCs to decrease apoptosis. In addition, the enhanced expression of YAP at the protein level as well as YAP/TEAD target genes, such as CTGF, ANKRD1, and the increase of YAP into the nucleus in immunofluorescence staining after the addition of EnSC-Exos to cisplatin-damaged GCs confirmed the suppression of Hippo signaling, While *in vivo*, EnSC-Exos successfully remedied POF in mice.

Conclusions

Collectively, our findings suggest that human EnSC-Exos is effective in recovery of ovarian function by chemotherapy-induced POF via activating YAP and inhibiting the Hippo signaling pathway. These findings provide new insights for further understanding of EnSC-Exos in the recovery of ovary function.

Background

Premature ovarian failure (POF), also known as primary ovarian insufficiency (POI), refers to women who are under the age of 40 years old, has amenorrhea, hypogonadotropic hypogonadism, and infertility (1). The main causes of POF include idiopathic factors such as genetics, immunity, and iatrogenic (chemotherapy and radiotherapy). POF is a devastating diagnosis for reproductive-aged women (2). With the improvement of chemotherapy drugs, the survival rate of cancer patients has been significantly improved, but gonadal damage is still a major complication, and the problem of ovarian damage caused by chemotherapy drugs needs to be resolved urgently (3). Due to stem cells having self-renewal and regeneration potential, they are considered to be effective in treating ovarian failure (4). Many studies have demonstrated that stem cells have great potential in treating infertility caused by female ovarian failure in various animal models and clinical studies (5–7). However, the quality, dosage and delivery route of stem cells must be carefully evaluated (8, 9). Stem cells secrete soluble factors, including extracellular vesicles (EVs), which may influence the microenvironment through paracrine mechanisms (10). Exosomes are nano-scale vesicles that can be used as a medium for cell-to-cell communication (11). In fact, several studies have revealed that exosomes have anti-inflammatory, anti-aging and wound healing effects *in vitro* and *in vivo* models (12). Compared with stem cells, exosomes are more convenient to save and transport. Moreover, they avoid many risks associated with cell transplantation (13). Evidence is mounting that stem cell-derived exosomes can also inhibit ovarian damage and alleviate the age-related fertility decline in female mice (14). However, the cellular and molecular mechanisms, including the signaling pathways, for improving ovarian function of exosomes need to be further elucidated.

The Hippo pathway was initially found in the fruit fly drosophila as an intrinsic mechanism that regulates organ size during development and is highly evolutionarily-conserved from drosophila to mammals (15). The Hippo pathway is a growth-supressive kinase cascade that restricts size during development. The core components of the Hippo pathway in mammals consists of a kinase cascade: sterile 20-like kinases (MST1/2), large tumour suppressor kinases (LATS1/2), transcriptional activator Yes-associated protein (YAP) and transcriptional co-activator with PDZ-binding motif (TAZ) (16). MST1/2 can bind to and phosphorylates Sav which is a regulatory, WW-domain containing protein that promotes Lats1/2 phosphorylation, Lats1/2 itself is also a kinase, which phosphorylates and inactivates YAP. The phosphorylated YAP is inactive since it binds to the cytoplasmic scaffold protein 14-3-3, which prevents its nuclear translocation, otherwise, it enters the nucleus via the nuclear pore, and from there can regulate gene expression (17, 18). Recent studies have revealed the Hippo signaling pathway might contribute to development, such as the Hippo signaling is inactivated and YAP and TAZ are activated and free to translocate into the nucleus to regulate target genes involved in cell proliferation, tissue growth, control of organ size and shape or metastasis as mention previously (19). Notably, Hippo pathway is important in folliculogenesis or ovarian function by regulating follicle activation and survival (20), further investigation revealed that enhanced YAP expression also contributed to massive primordial follicle activation (21). Study shows that disruption of Hippo signaling in the ovary promotes ovarian follicle growth through induction of CCN2 expression (22). At the same time, it has been suggested that disruption of Hippo

pathway by BMSCs in ovaries of radiation exposed rats which showed significant increase in YAP1, TEAD1 genes (23).

Here, we investigated the exogenous EnSC-Exos repressed apoptosis in cisplatin-induced GCs through activating YAP *in vitro* and effectively relieved follicles from atresia in POF mice model through Hippo pathway. Our study indicates the therapeutic potential of EnSC-Exos in chemotherapy-induced POF and the importance of Hippo pathway for POF treatment and thus provides more possible targets for treating POF.

Methods

Isolation of EnSCs

Human endometrial tissues were acquired from the Department of Obstetrics and Gynecology, the First Affiliated Hospital of Xi'an Jiaotong University (Xi'an, Shaanxi, China). This study was approved by the Ethical Committee of the First Affiliated Hospital of Xi'an Jiaotong University and the participants have written an informed content. Human endometrial stem cells (EnSCs) were cultured and identified as our previous study described (24). The tissue is placed in glassware under aseptic conditions and cut into $1mm^3$ with ophthalmic scissors and then digested by collagenase type I for 1 hours in a 37℃ rotating shaker. The digestion was terminated using Dulbecco's Modified Eagle Medium/Nutrient Mixture F12 (DMEM/F12, HyClone, USA) complete media and filtered with 200 mesh screen, 400 mesh screen. Finally, the cell-debrispellet was obtained by centrifugation at 800g for 5 minutes. Images of representative fields were visualized via a microscope (Olympus Corporation, Tokyo, Japan).

Cell culture

KGN cells were obtained from Wuhan Procell (Procell Life Science&Technology Co., Wuhan, China). Cell lines (KGN, EnSCs) were cultivated in DMEM/F12 supplemented with 10% fetal bovine serum (FBS, SiJiqing, China). Cells were cultured in a 5% CO_2 humidified incubator at 37℃. Human EnSCs were not maintained in culture for longer than 5 passages to ensure passage number remained fit for purpose.

Exosomes isolation, characterization and labeling

Exosomes were obtained from human EnSCs supernatants by differential centrifugation. The medium was discarded when EnSCs reached 80% confluency. Then, the cells were cultured in DMEM/F12 with 10% exosome-depleted FBS (VivaCell, cat. no.: C3801-0050, VivaCell Biosciences, Shanghai, China) for another 48 h. The supernatants were collected and then cleared by sequential centrifugation at 300 g for 10 min, 2000 g for 10 min and 10,000 g for 30 min at 4°C to filter cells and debris. The supernatants were ultracentrifuged at 120,000 g for 90 min to remove the supernatant (Beckman OptimaTM L-80 XP, Beckman Coulter, USA). Then precipitate was washed using phosphate-buffered saline (PBS) after which we centrifuged the supernatant at 120,000 g for 90 min at 4°C. Then, the precipitate was suspended in pre-cooled PBS to filtrate through 0.22-mm filters (Millipore, Billerica, MA, United States) (25). The

exosome concentrations were determined with a BCA protein assay kit (Proandy, cat. no.:10136-1, Proandy Biotechnology, Shaanxi, China).

To confirm the successful isolation of exosomes, western blotting was performed to detect the exosome marker proteins anti-HSP70 (dilution 1:500, cat. no.: sc-32239), anti-Alix (dilution 1:500, cat. no.: sc-53540) and anti-CD81 (dilution 1:500, cat. no.: sc-166029) from Santa Cruz (Santa Cruz Biotechnology, United States), anti-CD9 (D8O1A) (dilution 1:1000, cat. no.: #13174) and β-Actin (8H10D10) (dilution 1:5000, cat. no.: #3700) antibodies from Cell Signaling Technologies (Beverly, MA). Transmission electron microscopy (TEM, hitachi H-7650, Japan) was performed to verify the presence of exosomes. Exosomes were dissolved in PBS buffer, dropped onto a carbon-coated copper grid, and then stained with 2% uranyl acetate.

The EnSCs-Exos were labeled with PKH26 (Sigma-Aldrich, St. Louis, MO, USA) according to the manufacturer's instructions. In short, EnSC-Exos were incubated with red fluorescent dye (PKH26) for 4 min and treated with 0.5% BSA to neutralize redundant dye. Then, the labeled exosomes were obtained after centrifuged at 120,000 g for 90 min at 4°C to remove contaminating dye.

Induction of GC apoptosis *in vitro* and coculture of GCs and EnSC-Exos

Cisplatin (Sigma-Aldrich, St. Louis, MO) was used to make the cisplatin-induced granulosa cell injury model as previous (26). In order to clarify the function of exosomes to repair granulosa cells from cisplatin injury, 1×10^5 GCs were seeded into the of six-well plates and incubate for 24 h. Then the cisplatin was added to the GC culture medium at 10 μM to induce apoptosis. After exposure to cisplatin for 24 h (10 μM), the GCs were cocultured with EnSC-exosomes (200 μg/mL) or EnSC-exosomes (200 μg/mL) pretreated with Verteporfin (27) (1 μM, VP, a YAP inhibitor, catalog no.: HY-B0146, MedChemExpress, China) in the system for another 72 h.

For uptake of labeled exosomes, the cisplatin-induced granulosa cell injury model incubation with 10 μg/mL, 200 μg/mL PKH26-labeled exosomes for 24 h. Cells were washed twice with PBS and fixed in 4% paraformaldehyde for 10 min, thereafter, the nucleic was stained with 4', 6-diamidino-2-phenylindole (DAPI, Beyotime, cat. no.: P0131, Beyotime Biotechnology, Shanghai, China) and the cytoskeleton was stained with Actin-Tracker Green-488 (Beyotime, cat. no.: C2201S, Beyotime Biotechnology, Shanghai, China) according to the manufacturer's instructions. The uptake of PKH26-labeled exosomes by cisplatin-damaged GCs was detected by a fluorescence microscope (Nikon Ti-S, Nikon Corporation, Japan) and confocal laser scanning microscope (Leica TCS SP5 II, Leica Biosystems, Germany).

Immunofluorescence

Plant the cells on the slides and give them different treatments. Cells were washed twice with PBS, and fixed with 4% paraformaldehyde for 15 min. Then, cells were washed in PBS for three times and in 0.5% Triton X-100 (Beyotime, cat. no.: P0096, Beyotime Biotechnology, Shanghai, China) for 30 min. After that they were blocked with 5% BSA for 1 h. Next, they were incubated with primary antibodies (anti-YAP,

dilution 1:100, cat. no.: 13584-1-AP, Proteintech, USA), secondary antibodies (Invitrogen) and DAPI (Beyotime, cat. no.: P0131, Beyotime Biotechnology, Shanghai, China). Using a fluorescence microscope (Nikon Ti-S, Nikon Corporation, Japan), images were captured.

Western blot analysis and antibodies

Cell lysates (total protein) were collected using RIPA lysis buffer and detected the protein concentration with a BCA kit. According to the manufacturer's instructions, cell lysates were separated by 10% Bis-Tris Gels, under 72 V electrophoresis for 40 min, followed by 90 V electrophoresis for 90 min. After electrophoresis, proteins were transferred to NC membranes (PALL, Germany), under 320 mA for 100 min. After blocking with 5% non-fat milk or 5% BSA in TBS with 0.1% Tween-20 for 90 min at room temperature, the membranes were incubated with primary antibody overnight at 4℃. The next day, the membrane was then washed with Tris-Buffered Saline and Tween (TBST) for 30 min, the membranes were incubated with HRP-labeled secondary antibodies (dilution 1:3,000, cat. no.: ZB-2301, ZSGB-BIO, China) for 1.5 h, then the membrane was washed three times with TBST, chemiluminescence detection reagent was used to develop Chemiluminescent Imager (Tanon-5200). Gel image system was used to analyze the band density (Bio-Rad Laboratories, Inc). All protein expression levels were normalized to the level of the internal standard control GAPDH (dilution 1:4,000, cat. no.: AP0063, Bioworld Technology, USA). The following antibodies were used for immunoblotting: anti-Bcl-2 (dilution 1:1,500, cat. no.: 12789-1-AP), anti-Bax (dilution 1:1,500, cat. no.: 50599-2-Ig), anti-MST1 (dilution 1:1,000, cat. no.: 22245-1-AP), anti-LATS1 (dilution 1:1,500, cat. no.: 17049-1-AP) from Proteintech Group (Proteintech, USA), anti-Phospho-MST1 (Thr183)/MST2 (Thr180) (E7U1D) (dilution 1:1,000, cat. no.: #49332) antibody and anti-YAP (D8H1X) (dilution 1:1,000, cat. no.: #14074), anti-Phospho-YAP (Ser127) (D9W2I) (dilution 1:1,000, cat. no.: #13008), anti-Phospho-LATS1 (Ser909) (dilution 1:1,000, cat. no.: #9157), anti-CD9 (D8O1A) (dilution 1:1000, cat. no.: #13174) and β-actin (8H10D10) (dilution 1:5000, cat. no.: #3700) antibodies from Cell Signaling Technologies (Beverly, MA), anti-PCNA (dilution 1:500, cat. no.: sc-56), anti-Caspase-3 (dilution 1:500, cat. no.: sc-7272), anti-HSP70 (dilution 1:500, cat. no.: sc-32239), anti-Alix (dilution 1:500, cat. no.: sc-53540) and anti-CD81 (dilution 1:500, cat. no.: sc-166029) from Santa Cruz (Santa Cruz Biotechnology, United States).

RNA extraction and quantitative real-time PCR (qRT-PCR)

Total RNA was extracted using TRIzol reagent (Invitrogen, USA), and only highly pure RNAs (1.7 < A260/A280 < 2.2) were used. RNA (1 μg) was converted into cDNA using the PrimeScript™ RT reagent Kit with gDNA Eraser (Takara, Japan). After 10-fold dilution, 1000μg of cDNA was subjected to PCR amplification using TB Green® Premix Ex Taq™ II (Takara) according to the manufacturer's protocol in a Bio-Rad CFX Manager. The following thermocycling conditions were used for qPCR: 95℃ for 1 min, then 39 cycles with 95℃ for 20 sec, 60℃ for 20 sec, 72℃ for 30 sec. Glyceraldehyde-3-phosphate dehydrogenase (GAPDH) was used as an internal control. The expressions of genes were quantified using the $2^{-\Delta\Delta Cq}$ method. The primer sequences were as follows:

ANKRD1-F: 5’-GCCAAAGACAGAGAAGGAGATAC-3’,

ANKRD1-R: 5’-GAGATCCGCGCCATACATAAT-3’,

CYR61-F: 5’-CACACCAAGGGGCTGGAATG-3’,

CYR61-R: 5’-CCCGTTTTGGTAGATTCTGG-3’,

CTGF-F: 5’-GGAAATGCTGCGAGGAGTGG-3’,

CTGF-R: 5’-GAACAGGCGCTCCACTCTGTG-3’,

GAPDH-F: 5'-GTGAAGGTCGGAGTCAACGG-3’,

GAPDH-R: 5'-GAGGTCAATGAAGGGGTCATTG-3’.

Flow cytometry assay

Cisplatin-induced granulosa cells apoptosis and EnSC-Exos repair of the cisplatin-induced granulosa cell injury model were determined by flow cytometry using a Annexin V-FITC Apoptosis Detection Kit (BD Biosciences, CA, USA) according to the manufacturer’s protocol. Briefly, cells were washed two times with cold PBS and stained with Annexin V-FITC (5 μL) and propidium iodide (5 μL) for 15 min at room temperature (in darkness). The stained cells were analyzed using flow cytometry (FC 500, MCL, CA).

5-ethynyl-2'-deoxyuridine (EdU) labelling staining

To assess appropriate concentration for EnSC-Exos contribute to cisplatin-damaged GCs repair and the proliferation rate of the cisplatin-induced granulosa cell injury model in different groups, BeyoClick^{TM} 5-ethynyl-2-deoxyuridine (EdU)-594 kit (Beyotime, cat. no.: C0078S, Beyotime Biotechnology, Shanghai, China) was used according to the manufacturer’s instructions. In brief, KGN cells ($1×10^4$) were cultured in a 96-well plate for 24 h, the cisplatin was added to the GCs culture medium at 10 μM for 24 h to induce apoptosis (the cisplatin-induced granulosa cell injury model), then 100, 200, 400 μg/mL EnSC-Exos were suspended in cisplatin-damaged GCs for 72 h to detect the appropriate concentration for EnSC-exos contribute to cisplatin-damaged GCs repair. To detect the effect of Hippo pathway inhibitor on KGN proliferation in different groups, the GCs were cocultured with EnSC-exosomes (200 μg/mL) or EnSC-exosomes (200 μg/mL) pretreated with Verteporfin (1 μM) in the system for 72 h.

For EdU labelling assay, cells were incubated with EdU (1:1000, 10 μmol/L) for 2 h. Then, KGN cells was fixed with 4% formaldehyde for 15 minutes. Next, permeabilized the cells in 0.5% Triton X-100 (100 μL) for 15 minutes and added the BeyoClick^{TM} Labeled-Azide reaction cocktail (100 μL) for 30 minutes under light-shading conditions at room temperature. Finally, cells were counterstained with Hoechst 33342 (nuclear staining) for 30 minutes at room temperature. After 3 times washes with PBS, the images were acquired using luorescence microscope (Nikon Ti-S, Nikon Corporation, Japan). The proliferation rate of cells was assessed with the proportion of EdU-positive nucleus (red) to blue fluorescent nucleus.

Experimental animals, POF model establishment

To establish the POF model in mice, C57BL/6 female mice, aged 6-8weeks, body weight 16-18g, were purchased from Beijing Vital River Laboratory Animal Technology Co., Ltd. All experimental procedures were approved by the Ethical Committee and the Institutional Animal Care and Use Committee of Xi'an Jiaotong University. The mice were bred in a free condition in which the temperature is at 22-25℃ with water and food available ad libitum.

To establish the POF model, mice were injected with cisplatin (2 mg/kg) intraperitoneally for 10 consecutive days (5). To demonstrat the therapeutic effect of EnSC-Exos on POF ovarian function through Hippo pathway, the mice were randomly divided into 4 groups: (1) Control group (n = 10), (2) Cisplatin group (n = 10), cisplatin (2 mg/kg) intraperitoneal injection daily for 10 days, (3) Exosome group (n = 10), cisplatin (2 mg/kg) intraperitoneal injection daily for 10 days, exosome (350 μg/mouse) tail vein injection every other day on 11^{th} day for 12 days, (4) Verteporfin group (n = 10), cisplatin (2 mg/kg) intraperitoneal injection daily for 10 days, Verteporfin (75 mg/kg) intraperitoneal injection every other day on 11^{th} day for 4 times and exosome (350 μg/mouse) tail vein injection every other day on 11^{th} day at the same time for 12 days. The animals were euthanized by cervical dislocation after 22 days of treatment to collect serum and ovaries. We have recorded the body weight of each mouse every day (Figure 5A).

Enzyme Linked Immunosorbent Assay (ELISA)

After successful establishment of the POF mice model, the blood collected from the excised eyeball was transferred to a sterile tube for centrifugation at 3000 r/min for 10 minutes at 4℃, after which serum was obtained. Then, mice ELISA panel kits (Meimian Biotechnology, Jiangsu, China) were used to measure serum anti-Mullerian hormone (AMH), estradiol (E_2) and follicle stimulating hormone (FSH) levels according to the kit instructions.

Hematoxylin-eosin (HE) staining

The ovarian tissues were fixed in 4% paraformaldehyde for 24 h and then embedded in paraffin, finally cut into a 4-μm serial section. Then the tissue sections were rehydrated by incubating in xylene and subjecting to an alcohol gradient of 100%-70%. After deparaffinization, the section was stained with hematoxylin and eosin.

Immunohistochemistry (IHC)

The ovarian tissues of mice were fixed in 4% formaldehyde and paraffin-embedded using standard procedures. First, consecutive 4-μm sections were cut, deparaffinized with xylenes, rehydrated, and retrieved the antigen in sodium citrate solution (pH 6.0) for 20 minutes. Then the slides were treated with 3% hydrogen peroxide to quench the endogenous peroxidase and blocked with 1% bovine serum albumin (BSA) for 30 minutes to block the nonspecific binding. Next, tissue sections were incubated with primary antibody anti-YAP (dilution 1:200, cat. no.: 13584-1-AP, Proteintech, USA) overnight at 4℃. Finally, wash

the slides with PBS three times and incubate the slides with HRP-conjugated goat anti-rabbit IgG secondary antibody (1:1000, Santa, Cruze) for another 30 minutes. Finally, a 3, 3-diaminobenzidine tetrahydrochloride (DAB) (Beyotime, Shanghai, China) substrate kit was applied to detect peroxidase reactivity. According to the manufacturer instructions, we prepared DAB peroxidase substrate in 5 mL ddH_2O in a glass vial. Then, drop the DAB substrate on top of the slides and watch the brown staining. Dip slides into ice plus tap water to stop the reaction and rinse under cold tap water for 5 min.

Statistical analysis

The statistical analyses were carried out using GraphPad Prism software. All experiments were performed in triplicate and all results are presented as the mean ± SD. Analysis of differences between the two groups were performed using Student's t test, one-way ANOVA. Significance is indicated as follows: $^{*}P < 0.05$, $^{**}P < 0.01$.

Results

Cultivation and characterization of EnSC-Exos

EnSCs passaged three to five times had a uniform morphologica appearance as fibroblast-like long spindles in an ordered arrangement (Figure 1A). EnSCs possessing a multilineage differentiation capability and flow cytometry was used to identify the expression of surface markers as mention previously (28). EnSC-Exos were isolated by differential ultracentrifugation. Based on protein content, the average production of exosomes was approximately 10 μg/μL. Characteristics of EnSC-Exos were analyzed by electron microscopy, which revealed vesicular structures-circular and double membrane wrapped in shape. At the same time, electron microscopy analysis showed that the size was range 60-250 nm (Figure 1B). Western blot revealed the presence of exosome surface markers including Alix, HSP70, CD81 and CD9 (Figure 1C). This infers that human EnSC-Exos were successfully isolated.

Cisplatin-damaged GCs induce the apoptosis *in vitro* through activating the Hippo signaling pathway

Cisplatin is one of the most potential and widely used drugs for the treatment of various solid cancers such as ovarian, cervical cancer and several others (29). In order to be closer to the actual situation, we chose cisplatin to induce apoptosis of granulosa cells to establish the cisplatin-induced granulosa cell injury model *in vitro* for subsequent experiments. Using 0, 5, 10 or 20 μM of cisplatin concentration induced granulosa cells apoptosis for 24 h was determined by flow cytometry. After staining the GCs in each group with Annexin V-FITC and propidium iodide, the apoptotic GCs were counted. Figure 2A showed the apoptosis rate of cisplatin-damaged GCs was increased in a dose dependent manner in the concentration range of 0-20 μM. Western blot showed cisplatin efficiently stimulated cell apoptosis in a dose dependent manner and the level of apoptosis protein Bax, Caspase-3 was remarkably up-regulated but the expression of anti-apoptosis protein Bcl-2 was distinctly down-regulated in cisplatin-damaged GCs, which leaded to the higher ratio of Bax/Bcl-2 (Figure 2B). These results suggest 10 μM was selected as the optimal concentration for subsequent experiments as mention previously (26).

MST and LATS are core kinase cascades of the Hippo pathway while YAP and TAZ are downstream effector. When Hippo signaling is activated, MST phosphorylates and activates LATS in mammalian cells. Then, activated LATS phosphorylates YAP at S127, providing a docking site for 14-3-3 proteins, sequestering YAP in the cytoplasm (30). In nucleus, YAP/TAZ interacts significantly with TEA DNA-binding proteins transcription factors and forms the YAP/TAZ-TEAD complex that mediates proliferative and prosurvival genes such as the connective tissue growth factor (CTGF), cysteine-rich angiogenic inducer 61 (CYR61), Ankyrin repeat domain 1 (ANKRD1), and others to promote cell survival, proliferation, and growth (31). In contrast, unphosphorylated YAP translocates into the nucleus, where it acts as a transcriptional coactivator to induce expression of genes that promote cell proliferation and inhibit apoptosis.

For the purpose of determining whether the expression level of the Hippo pathway core effectors was associated with the cisplatin-induced granulosa cell injury model, we measured the protein levels of phospho-MST1 (p-MST1), p-LATS1 (the active form), p-YAP (the inactive form), MST, LATS1 and YAP (the active form) by western blot analysis as well as the levels of YAP by immunofluorescence, while the YAP target genes were measured by qRT-PCR. We found that treatment of GCs with cisplatin *in vitro* reduced the protein expression levels of LATS1, YAP, and MST and increased the expression levels of p-LATS1, p-YAP, and p-MST1 in a time-dependent manner (Figure 2C). Using qRT-PCR, we found that the total RNA levels of the YAP target genes ANKRD1, CTGF and CYR61 were also decreased after cisplatin treatment (Figure 2D).

Furthermore, immunofluorescence staining revealed that expression of YAP had a lower level of cytoplasm expression and nucleus accumulation in the cisplatin-damaged GCs, compared to the control group. In addition, the expression level of YAP is decreased as the concentration of cisplatin increases and there is almost no expression of YAP in the cytoplasm and nucleus of 20 μM cisplatin-damaged GCs (Figure 2E). Therefore, these results suggest that cisplatin damage GCs and suppress proliferation of GCs by activating the expression of Hippo/YAP signaling core effectors.

Uptake of EnSC-Exos by cisplatin-damaged GCs *in vitro*

The appropriate concentration for EnSC-exos contribute to the cisplatin-induced granulosa cell injury model (the cisplatin was added to the GCs culture medium at 10 μM for 24 h to induce apoptosis) repair was determined by EdU assay. The results showed that the proliferation rate of cisplatin-damaged GCs treated with 200 or 400 μg/mL EnSC-Exos for 72 h was significantly higher when compared to the 100 μg/mL EnSC-Exos. Thereby, 72 h of incubation with 200 μg/mL EnSC-Exos significantly promoted the proliferation of cisplatin-damaged GCs and were used for subsequent experiments (Figure 3A).

Exosomes are known to be taken up by other cells by endocytosis, triggering cellular responses (32). EnSC-Exos were labeled with PKH26, a fluorescent cell linker compound. To evaluate the internalization of EnSC-Exos, cisplatin-damaged GCs *in vitro* were incubated with 200 μg/mL and 10 μg/mL PKH26 labeled EnSC-Exos for 24 h, which can be observed strong red fluorescence under the fluorescence microscope in the cytoplasm of cells (Figure 3B). Furthermore, when the exosomes concentration was 10

μg/mL, the uptake could be seen by immunofluorescence microscopy in the cisplatin-induced granulosa cell injury model. While under the concentration of 200 μg/mL, EnSC-Exo increased the uptake of fluorescence intensity in cisplatin-damaged GCs. Confocal laser scanning microscope showed clearly that 10 μg/mL PKH26 labeled human EnSC-Exos were located inside the cytoplasmic compartment of cisplatin-damaged GCs (Figure 3 C).

In addition, the red fluorescence decreases after the addition of Hippo pathway inhibitor Verteporfin at 1 μM (Figure 3 B). Verteporfin (VP) is a suppressor of YAP, used as a photosensitizer for photodynamic therapy in patients with age-related macular degeneration (33). These results suggested that EnSC-Exos could be taken in by cisplatin-damaged GCs and the endocytosis of exosomes was reduced after inhibiting the Hippo signaling pathway *in vitro*.

EnSC-Exos attenuated the apoptosis on cisplatin-damaged GCs by suppressing Hippo pathway *in vitro*

The biological function of EnSC-Exos contributed to cisplatin-damaged GCs was analysed using flow cytometry analysis, western blot and EdU labelling assay. In our research, the apoptosis rates of positive control (Cisplatin group) were significantly higher than negative control (Control group). The apoptosis rate of cisplatin-damaged GCs cocultured with EnSC-Exos (200 μg/mL) for 72 h was decreased, there was significant difference among Cisplatin group and Exosome group, contemporary (Figure 4A). Western blot showed that EnSC-Exos could inhibit the expression of apoptosis protein Bax and promote the expression of proliferation protein PCNA in cisplatin-damaged GCs, the anti-apoptotic effect of EnSC-Exos is reduced after adding Hippo pathway inhibitors -Verteporfin (Figure 4B). Afterwards, proliferation of EnSC-Exos induced cisplatin-damaged GCs was evaluated by EdU labelling assay. The result showed that EnSC-Exos (200 μg/mL) enhanced cell proliferation of the cisplatin-induced granulosa cell injury model. As expected, EnSC-Exos induced growth of cisplatin-damaged GCs was significantly inhibited by the addition of Hippo pathway inhibitor Verteporfin at 1 μM (Figure 4C). All results indicate that human EnSc-Exos could promote the repair of the cisplatin-induced granulosa cell injury model which was associated with Hippo pathway.

Next, the mechanism underneath of Hippo pathway in the therapeutic effects of EnSC-Exos on cisplatin-damaged GCs was detected using western blot analysis, qRT-PCR and immunofluorescence staining. KGN cell lines were maintained in cisplatin (10 μM) for 24 h to establish cisplatin-induced granulosa cell injury model. Then cisplatin-damaged GCs treated with PBS (Cisplatin group), EnSC-Exos (200 μg/mL) (Exosome group) or EnSC-Exos (200 μg/mL) with Verteporfin (1 μM) (Exosome + Verteporfin group) for another 72 h. Western blot indicated that cisplatin could induce YAP phosphorylation, while EnSC-Exos up-regulated the protein expression level of YAP and then decreased phosphorylation of YAP. What is more interesting, cells were treated with Verteporfin and EnSC-Exos for 72 h, the expression of proteins in the Hippo pathway, such as total YAP, p-YAP, LATS1, p-LATS1 and MST1 were inhibited. The results indicate that EnSc-Exos may inhibit cisplatin-damaged GCs apoptosis via the Hippo pathway (Figure 4D). Using qRT-PCR, we found that the total RNA levels of the YAP target genes ANKRD1 and CTGF were increased after EnSc-Exos treatment, while decreased in Exosome and Verteporfin group (Figure 4E).

As shown in Figure 4F, cisplatin could induce YAP phosphorylation and cytoplasmic localization, which was, as expected, decrease nuclear localization, confirming the Hippo pathway was involved in the apoptotic effect of cisplatin-induced granulosa cells. In contrast, EnSC-Exos caused YAP translocated into nucleus. On the other hand, the inhibitor of Hippo pathway (Verteporfin) significantly suppressed exosomes-induced YAP nuclear localization. Taken together, our observations support a physiological role of EnSC-Exos on cisplatin-damaged GCs in Hippo pathway regulation, which means EnSC-Exos could inhibit cell apoptosis in cisplatin-damaged GCs via suppresses the Hippo pathway.

Therapeutic effects of Human EnSC-Exos on premature ovarian failure mice

Mice were injected intraperitoneally with 2 mg/kg cisplatin daily for 10 days to establish the POF model(5). Control group did not receive cisplatin. On the eleventh day of cisplatin administration, mice were randomly divided into three groups: (1) received PBS (POF group). (2) hEnSC-Exos (passage 3~5, 350 μg/mouse) every other day on 11^{th} day by tail vein injection (Exosome group). (3) Verteporfin (75 mg/kg) intraperitoneal injection for 4 times as well as human EnSC-Exos tail vein injection every other day on 11^{th} day at the same time (Verteporfin group). After 12 days, mice were weighed and sacrificed (Figure 5A). As shown in Figure 5B, six days after injection, Exosome group showed significantly increased body weight compared to POF and Verteporfin groups. Body weight from verteporfin-treated mice and POF group were significantly lighten than those from exosome-treated on 12 days after therapeutic. Furthermore, following human EnSC-Exos injection, the serum levels of anti-Mullerian hormone (AMH), estradiol (E_2) were increased but follicle stimulating hormone (FSH) levels were decreased in Exosomes group compared with POF group, while when incorporation of verteporfin during EnSC-Exos repairing in POF model can reduce E_2 and AMH levels and increase FSH levels in the serum (Figure 5C).

To further examine the effects of human EnSC-Exos transplantation on ovarian function, ovaries were analyzed by histologically. In the Control group, the ovaries contained numerous healthy follicles at different stages. In contrast, mice in the cisplatin-treated chemotherapy group showed atrophied ovaries composed of interstitial cells in a fibrous matrix. POF group demonstrated that a significant reduction in the number of primordial, primary, secondary, and mature follicles. Interestingly, injected with human EnSC-Exos significantly inhibited granulosa cell apoptosis, protected the ovarian vasculature from damage, and were increased in total number of healthy follicles and decrease of atresia follicles. What's more, the morphology of ovarian sections showed that abnormal structural, interstitial hyperplasia, severe fibrosis, and less number of functional follicles were observed in in veterporfin-treated mice compared with the Exosome group (Figure 5D). Because the activation of follicles depends on the Hippo pathway, we detected the expression of YAP proteins in the different treatment groups. Immunohistochemical analysis showed that chemotherapy significantly decreased YAP protein expression in ovaries. However, human EnSC-Exos slightly enhanced YAP expression in injured ovaries, while verteporfin decreased the expression of YAP (Figure 5D). These results indicate that EnSC-Exos have the potential to repair ovarian function in POF mice model through Hippo pathway.

Discussion

Approximately 10% of cancers are present in women under 45 years of age (34). Treatments for cancer of the female reproductive system, such as cisplatin-based chemotherapy, induces ovarian damage, including granulosa cell apoptosis, ovarian vascular damage, rapid depletion of the follicle reserve, resulting in POF, which also known as ovarian function insufficient (POI) (35). However, though known to cause intermediate gonadal toxicity, no radical cure is yet available for reversing the chemotherapy-induced damage to the ovarian structure and function in women of reproductive age (36). Within the normal ovary, oocytes are stored in the form of primordial follicles, surrounded by somatic granulosa cells. What's more importantly, granulosa cells play a critical role in follicular activation and follicular function. Excessive apoptosis of granulosa cells is a key mechanism for follicular atresia (37). It suggests that promoting proliferation of GCs can rescue cisplatin-damaged ovarian structures and functions. Various approaches were used to preserve fertility in women with cancer, such as embryo cryopreservation, mature-oocyte cryopreservation after ovarian stimulation or ovarian tissue, transplantation, and ovarian protection with GnRH-a (34). However, more studies are required to evaluate feasibility, safety, and efficacy of these fertility-preserving methods and identify better therapeutic strategies to rescue the function of ovarian in chemotherapy.

With the development of regenerative medicine, human stem cell therapy brings new prospects for POF. Since stem cells have strong self-renewal and regeneration potential, they can be used in treatment of ovarian failure. To date, many studies point to the efficacy of stem cells in POF animal model treatment, such as mesenchymal stem cells (MSCs), stem cells from extra-embryonic tissues, induced pluripotent stem cells (iPSCs) and ovarian stem cells (38). Although numerous experimental studies have been developed, clinical applications of stem cells have limitations, including insufficient cell sources, immunogenicity, subculture, and ethical issues (39). It is very urgent to identify the effective components of stem cells in the treatment of POF to avoid potential side effects. Hence, the cell-free therapy, which was used stem cells as a source of therapeutic molecules, could be developed to treat POF disease models. Exosomes secreted by stem cells, which function as messengers between cells, have been studied on the biological effects because they are smaller and easier to produce and have no risk of tumor formation (40). Recently, many studies have reported that exosomes play a key role in stem cell-mediated tissue functional repair. For example, human amniotic epithelial cell-derived exosomes (hAEC-exosomes) increased the number of follicles and improved ovarian function in POF mice. During the early stage of transplantation, hAEC-exosomes significantly inhibited granulosa cell apoptosis, protected the ovarian vasculature from damage, and were involved in maintaining the number of primordial follicles in the injured ovaries *in vivo* (41). In the present study, we characterized exosomes secreted by human EnSC in vitro (Fig. 1). The uptake of EnSC-Exos by cisplatin-damaged GCs was observed by immunofluorescence staining and laser scanning confocal microscope, confirming direct interaction between exosomes and damaged cells (Fig. 3). We also provide new evidence that the expression of PCNA was significantly up-regulated by treating the cisplatin-damaged GCs with EnSC-Exos which means exosomes treatment brings about sustained changes in the proliferation and anti-apoptosis of cisplatin-damged cells (Fig. 4).

Several studies demonstrated that granulosa cell apoptosis was a causative factor accelerating follicular depletion and atresia depending on the Hippo pathway, which was also negatively regulated by follicle development. Research demonstrated that chemotherapy treatment led to the abnormal of Hippo signaling pathway in ovaries, which were related to the primordial follicle loss and granulosa cell apoptosis. Study demonstrated the expression of Hippo signaling pathway genes and showed that ovarian fragmentation increased actin polymerization, leading to YAP nuclear translocation and enhancing follicle growth in the mammalian ovary (22). Further investigation revealed that enhancing YAP expression and an increased pro-inflammatory response also contributed to massive primordial follicle activation (42). Previous studies showed that Hippo signaling pathway was mainly involved in the regulation of ovarian fragmentation which means that ovarian development is closely related to the Hippo pathway (43). Consistent with this, Hippo is down-regulated in many ovarian damaged cells, we propose that EnSC-exosomes treatment attenuates ovarian damage and restores ovarian function in POF which was related to Hippo pathway. To our knowledge, this is the first study to investigate the interaction between human EnSC-Exos which are related to Hippo pathway in POF model (Fig. 6). In order to dicover the beneficial effects of EnSC-Exos in restoring ovarian function in POF and the potential mechanisms. We observe the conditions of cisplatin-damaged CGs treated with exosomes or Hippo pathway inhibitor (Verteporfin). The results showed that cell apoptosis decreased under EnSC-Exos and this effect was reversed by Verteporfin. Subsequently, the cytoplasmic and nuclear fractions were isolated to evaluate the translocation of YAP in cisplatin-treated CGs. After exosomes treatment, the translocation from cytoplasmic to nuclear of YAP protein was increased while Hippo pathway inhibitor were decreased.

In addition, we established a POF mice model to further verify the experimental results. We explored the dose of injection of verteporfin during the animal experiment. The mice in the Verteporfin group died on the second day when we used 100 mg/kg in POF model as studies showed (44–46), which was considered as there was superimposed toxic effects when using verteporfin and cisplatin, the body weight of Verteporfin group did not decrease significantly when we used 50 mg/kg verteporfin compared with the exosomes group according to the literature (47). The reason was considering as that it was impossible to block Hippo pathway because of the low dose. Therefore, we selected 75 mg/kg Verteporfin to establish the POF mice model. The mental state was poor while the body weight was low in the Verteporfin group after the fourth injection. We thought that it was not suitable to continue to inject verteporfin. In order to observe whether exosomes play a role in ovarian repair after blocking the Hippo pathway, exosomes were injected as usual in order to observe whether verteporfin could continue to block the Hippo pathway after stopping injection as well as exosomes had the ability to repair ovarian function (Fig. 5A&B). The abnormal structure, severe fibrosis was observed in the ovary tissues of Verteporfin group and POF group. In contrast, the morphology and structure of the ovary tissues showed recovery with the evidence of decreased fibrosis and increased number of functional follicles at all developmental stages after EnSC-Exos injection (Fig. 5C). Since the verteporfin was injected only four times whereas the exosomes continued to be injected in the Verteporfin group, it could be seen that there were new follicles in the ovary (Fig. 5C&D). Immunohistochemistry showed that the expression of YAP increased in the Control and Exosomes groups while decreased in Cisplatin and Verteporfin groups. Based on these

results, we demonstrated that exosomes to suppress the Hippo pathway and increases YAP activation to result in anti-apoptosis of cisplatin-damaged CGs and POF model. In our research, all these data provide a potential therapeutic approach to treatment with ovarian injury. However, our study still has some limitations. First, it is needed to verify in a large number of animal experiments whether the dose and time of verteporfin used in cisplatin-induced POF mice model affect the blocking effect of Hippo pathway. Second, regardless of the fact that we observed exosomes could be used in cisplatin-damaged CGs, the molecular mechanism underlying the upstream or the downstream signaling molecule such as RNA, protein and growth factors we did not further investigate. In addition, the therapeutic effect of EnSC-Exos remains to be validated in a clinical trial such as POF patients. All these limitations should be discussed in the future study.

Taken together, human EnSC-Exos were successfully isolated, identified and labeling. Furthermore, we found the Hippo signaling pathway was responsible for the apoptosis of cisplatin-damaged CGs. *In vitro*, co-cultured with EnSC-Exos significantly improved the proliferation levels of cisplatin-damaged GCs. Human EnSC-Exos injection can promote ovarian cells proliferation and restore ovarian function in POF mice model. Furthermore, we found that the therapeutic effect of EnSC-Exos on cisplatin-damaged GCs was inhibited by the Hippo pathway inhibitor-verteporfin in vitro and POF mice model.

Conclusions

Our research shows that human EnSC-Exos can repair ovarian injury, stimulate regeneration and recovery of ovarian function via activating YAP and inhibiting the Hippo signaling pathway. Our findings suggest that EnSC-exosomes could act as an additional mechanism contributing to follicles and improved ovarian function microenvironment which is related to Hippo pathway. Thus, human EnSC-Exos injection may provide an effective and novel method for treating chemotherapy-induced POF.

Abbreviations

AMH
anti-Mullerian hormone
ANKRD1
Ankyrin repeat domain 1
CTGF
connective tissue growth factor
CYR61
cysteine-rich angiogenic inducer 61
EVs
extracellular vesicles
E_2
Estradiol
EdU

5-ethynyl-2'-deoxyuridine
ELISA
Enzyme-linked immunosorbent assay
EnSCs
Endometrial stem cell
Exos
exosomes
EnSC-Exos
Endometrial stem cell-derived exosomes
FSH
follicle stimulating hormone
HE
Hematoxylin-eosin
IHC
Immunohistochemical
GCs
granulosa cells
GAPDH
glyceraldehyde-3-phosphate dehydrogenase
LATS1
large tumor suppressor 1
MSCs
Mesenchymal stem cells
MSC-exosomes
mesenchymal stem cell-derived exosomes
MST1
mammalian Ste20-like protein kinases 1
POF
Premature ovarian failure
POI
primary ovarian insufficiency
PBS
phosphate-buffered saline
qRT-PCR
quantitative real-time PCR
TAZ
transcriptional coactivator with a PDZ-binding domain
VP
Verteporfin
WB

Western blot
YAP
Yes-associated protein
p-YAP
phospho-YAP

Declarations

Ethics approval and consent to participate

The collection of the samples used for research purposes in this study was approved by the Ethical Committee of The First Affiliated Hospital of Xi'an Jiantong University, and written informed consent was obtained from each donor.

The experimental protocol about animals was approved by the Ethical Committee and the Institutional Animal Care and Use Committee of Xi'an Jiaotong University.

Consent for publication

Not applicable.

Availability of data and materials

All data generated or analysed during this study are included in this published article.

Competing interests

The authors declare that they have no competing interests.

Funding

This study was supported by "the National Natural Science Foundation of China (No. 81571393)", "Shaanxi Provincial Natural Science Foundation (No. 2019 KW-065)", and "Project A of the First Afliated Hospital of Xi'an Jiaotong University (XJTU-2021-02)".

Authors' contributions

YXY, WW, and WLJ were in charge of the conception, study design, and literature research. WLJ, WLH, WRL, and XT were in charge of the experimental studies. CZW, CFY and WJY were in charge of the experimental studies and data analysis/interpretation. WW, WLJ and WJY were in charge of manuscript preparation and editing and revision and final version approval of the manuscript. All authors read and approved the ending version of the final manuscript.

Acknowledgements

We thank the support of Center for Translational Medicine, the First Affiliated Hospital of Xi'an Jiaotong University, China. All authors are acknowledged for their contribution to the study.

References

1. Ghahremani-Nasab M, Ghanbari E, Jahanbani Y, Mehdizadeh A, Yousefi M. Premature ovarian failure and tissue engineering. J Cell Physiol. 2020;235(5):4217–26.
2. Blumenfeld Z. What Is the Best Regimen for Ovarian Stimulation of Poor Responders in ART/IVF? Front Endocrinol (Lausanne). 2020;11:192.
3. Cho HW, Lee S, Min KJ, Hong JH, Song JY, Lee JK, et al. Advances in the Treatment and Prevention of Chemotherapy-Induced Ovarian Toxicity. Int J Mol Sci. 2020;21(20).
4. Zhang C. The Roles of Different Stem Cells in Premature Ovarian Failure. Curr Stem Cell Res Ther. 2020;15(6):473–81.
5. Yoon SY, Yoon JA, Park M, Shin EY, Jung S, Lee JE, et al. Recovery of ovarian function by human embryonic stem cell-derived mesenchymal stem cells in cisplatin-induced premature ovarian failure in mice. Stem Cell Res Ther. 2020;11(1):255.
6. Bahrehbar K, Rezazadeh Valojerdi M, Esfandiari F, Fathi R, Hassani SN, Baharvand H. Human embryonic stem cell-derived mesenchymal stem cells improved premature ovarian failure. World J Stem Cells. 2020;12(8):857–78.
7. Ding L, Yan G, Wang B, Xu L, Gu Y, Ru T, et al. Transplantation of UC-MSCs on collagen scaffold activates follicles in dormant ovaries of POF patients with long history of infertility. Sci China Life Sci. 2018;61(12):1554–65.
8. Esfandyari S, Chugh RM, Park HS, Hobeika E, Ulin M, Al-Hendy A. Mesenchymal Stem Cells as a Bio Organ for Treatment of Female Infertility. Cells. 2020;9(10).
9. Shareghi-Oskoue O, Aghebati-Maleki L, Yousefi M. Transplantation of human umbilical cord mesenchymal stem cells to treat premature ovarian failure. Stem Cell Res Ther. 2021;12(1):454.
10. Batsali AK, Georgopoulou A, Mavroudi I, Matheakakis A, Pontikoglou CG, Papadaki HA. The Role of Bone Marrow Mesenchymal Stem Cell Derived Extracellular Vesicles (MSC-EVs) in Normal and Abnormal Hematopoiesis and Their Therapeutic Potential. J Clin Med. 2020;9(3).
11. Kim YG, Choi J, Kim K. Mesenchymal Stem Cell-Derived Exosomes for Effective Cartilage Tissue Repair and Treatment of Osteoarthritis. Biotechnol J. 2020;15(12):e2000082.
12. Ha DH, Kim HK, Lee J, Kwon HH, Park GH, Yang SH, et al. Mesenchymal Stem/Stromal Cell-Derived Exosomes for Immunomodulatory Therapeutics and Skin Regeneration. Cells. 2020;9(5).
13. Wu P, Zhang B, Shi H, Qian H, Xu W. MSC-exosome: A novel cell-free therapy for cutaneous regeneration. Cytotherapy. 2018;20(3):291–301.
14. Jiao W, Mi X, Qin Y, Zhao S. Stem Cell Transplantation Improves Ovarian Function through Paracrine Mechanisms. Curr Gene Ther. 2020;20(5):347–55.

15. Hong AW, Meng Z, Guan KL. The Hippo pathway in intestinal regeneration and disease. Nat Rev Gastroenterol Hepatol. 2016;13(6):324–37.
16. Ma S, Meng Z, Chen R, Guan KL. The Hippo Pathway: Biology and Pathophysiology. Annu Rev Biochem. 2019;88:577–604.
17. Meng Z, Moroishi T, Guan KL. Mechanisms of Hippo pathway regulation. Genes Dev. 2016;30(1):1–17.
18. Huang J, Wu S, Barrera J, Matthews K, Pan D. The Hippo signaling pathway coordinately regulates cell proliferation and apoptosis by inactivating Yorkie, the Drosophila Homolog of YAP. Cell. 2005;122(3):421–34.
19. Dey A, Varelas X, Guan KL. Targeting the Hippo pathway in cancer, fibrosis, wound healing and regenerative medicine. Nat Rev Drug Discov. 2020;19(7):480–94.
20. Gershon E, Dekel N. Newly Identified Regulators of Ovarian Folliculogenesis and Ovulation. Int J Mol Sci. 2020;21(12).
21. Kawamura K, Cheng Y, Suzuki N, Deguchi M, Sato Y, Takae S, et al. Hippo signaling disruption and Akt stimulation of ovarian follicles for infertility treatment. Proc Natl Acad Sci U S A. 2013;110(43):17474–9.
22. Hsueh AJW, Kawamura K. Hippo signaling disruption and ovarian follicle activation in infertile patients. Fertil Steril. 2020;114(3):458–64.
23. El-Derany MO, Said RS, El-Demerdash E. Bone Marrow-Derived Mesenchymal Stem Cells Reverse Radiotherapy-Induced Premature Ovarian Failure: Emphasis on Signal Integration of TGF-β, Wnt/β-Catenin and Hippo Pathways. Stem Cell Rev Rep. 2021;17(4):1429–45.
24. Wang Z, Wang Y, Yang T, Li J, Yang X. Erratum to: Study of the reparative effects of menstrual-derived stem cells on premature ovarian failure in mice. Stem Cell Res Ther. 2017;8(1):49.
25. Théry C, Amigorena S, Raposo G, Clayton A. Isolation and characterization of exosomes from cell culture supernatants and biological fluids. Curr Protoc Cell Biol. 2006;Chap. 3:Unit 3.22.
26. Wang R, Wang W, Wang L, Yuan L, Cheng F, Guan X, et al. FTO protects human granulosa cells from chemotherapy-induced cytotoxicity. Reprod Biol Endocrinol. 2022;20(1):39.
27. Wang L, Li J, Wang R, Chen H, Wang R, Wang W, et al. NGF Signaling Interacts With the Hippo/YAP Pathway to Regulate Cervical Cancer Progression. Front Oncol. 2021;11:688794.
28. Wang Z, Wang Y, Yang T, Li J, Yang X. Study of the reparative effects of menstrual-derived stem cells on premature ovarian failure in mice. Stem Cell Res Ther. 2017;8(1):11.
29. Ghosh S. Cisplatin: The first metal based anticancer drug. Bioorg Chem. 2019;88:102925.
30. Yuan P, Hu Q, He X, Long Y, Song X, Wu F, et al. Laminar flow inhibits the Hippo/YAP pathway via autophagy and SIRT1-mediated deacetylation against atherosclerosis. Cell Death Dis. 2020;11(2):141.
31. Dimri M, Satyanarayana A. Molecular Signaling Pathways and Therapeutic Targets in Hepatocellular Carcinoma. Cancers (Basel). 2020;12(2).

32. Gruenberg J, Stenmark H. The biogenesis of multivesicular endosomes. Nat Rev Mol Cell Biol. 2004;5(4):317–23.
33. Fusco P, Mattiuzzo E, Frasson C, Viola G, Cimetta E, Esposito MR, et al. Verteporfin induces apoptosis and reduces the stem cell-like properties in Neuroblastoma tumour-initiating cells through inhibition of the YAP/TAZ pathway. Eur J Pharmacol. 2021;893:173829.
34. Dolmans MM, Donnez J. Fertility preservation in women for medical and social reasons: Oocytes vs ovarian tissue. Best Pract Res Clin Obstet Gynaecol. 2021;70:63–80.
35. Meirow D, Nugent D. The effects of radiotherapy and chemotherapy on female reproduction. Hum Reprod Update. 2001;7(6):535–43.
36. Sonigo C, Beau I, Binart N, Grynberg M. The Impact of Chemotherapy on the Ovaries: Molecular Aspects and the Prevention of Ovarian Damage. Int J Mol Sci. 2019;20(21).
37. Quirk SM, Cowan RG, Harman RM, Hu CL, Porter DA. Ovarian follicular growth and atresia: the relationship between cell proliferation and survival. J Anim Sci. 2004;82 E-Suppl:E40-52.
38. Sheikhansari G, Aghebati-Maleki L, Nouri M, Jadidi-Niaragh F, Yousefi M. Current approaches for the treatment of premature ovarian failure with stem cell therapy. Biomed Pharmacother. 2018;102:254–62.
39. Fu YX, Ji J, Shan F, Li J, Hu R. Human mesenchymal stem cell treatment of premature ovarian failure: new challenges and opportunities. Stem Cell Res Ther. 2021;12(1):161.
40. Esfandyari S, Elkafas H, Chugh RM, Park HS, Navarro A, Al-Hendy A. Exosomes as Biomarkers for Female Reproductive Diseases Diagnosis and Therapy. Int J Mol Sci. 2021;22(4).
41. Zhang Q, Sun J, Huang Y, Bu S, Guo Y, Gu T, et al. Human Amniotic Epithelial Cell-Derived Exosomes Restore Ovarian Function by Transferring MicroRNAs against Apoptosis. Mol Ther Nucleic Acids. 2019;16:407–18.
42. Gao J, Song T, Che D, Li C, Jiang J, Pang J, et al. Deficiency of Pdk1 contributes to primordial follicle activation via the upregulation of YAP expression and the pro–inflammatory response. Int J Mol Med. 2020;45(2):647–57.
43. Ai A, Xiong Y, Wu B, Lin J, Huang Y, Cao Y, et al. Induction of miR-15a expression by tripterygium glycosides caused premature ovarian failure by suppressing the Hippo-YAP/TAZ signaling effector Lats1. Gene. 2018;678:155–63.
44. Chen J, Wang X, He Q, Bulus N, Fogo AB, Zhang MZ, et al. YAP Activation in Renal Proximal Tubule Cells Drives Diabetic Renal Interstitial Fibrogenesis. Diabetes. 2020;69(11):2446–57.
45. Song Y, Fu J, Zhou M, Xiao L, Feng X, Chen H, et al. Activated Hippo/Yes-Associated Protein Pathway Promotes Cell Proliferation and Anti-apoptosis in Endometrial Stromal Cells of Endometriosis. J Clin Endocrinol Metab. 2016;101(4):1552–61.
46. Jin J, Wang T, Park W, Li W, Kim W, Park SK, et al. Inhibition of Yes-Associated Protein by Verteporfin Ameliorates Unilateral Ureteral Obstruction-Induced Renal Tubulointerstitial Inflammation and Fibrosis. Int J Mol Sci. 2020;21:21.

47. Bottini A, Wu DJ, Ai R, Le Roux M, Bartok B, Bombardieri M, et al. PTPN14 phosphatase and YAP promote TGFβ signalling in rheumatoid synoviocytes. Ann Rheum Dis. 2019;78(5):600–9.

Figures

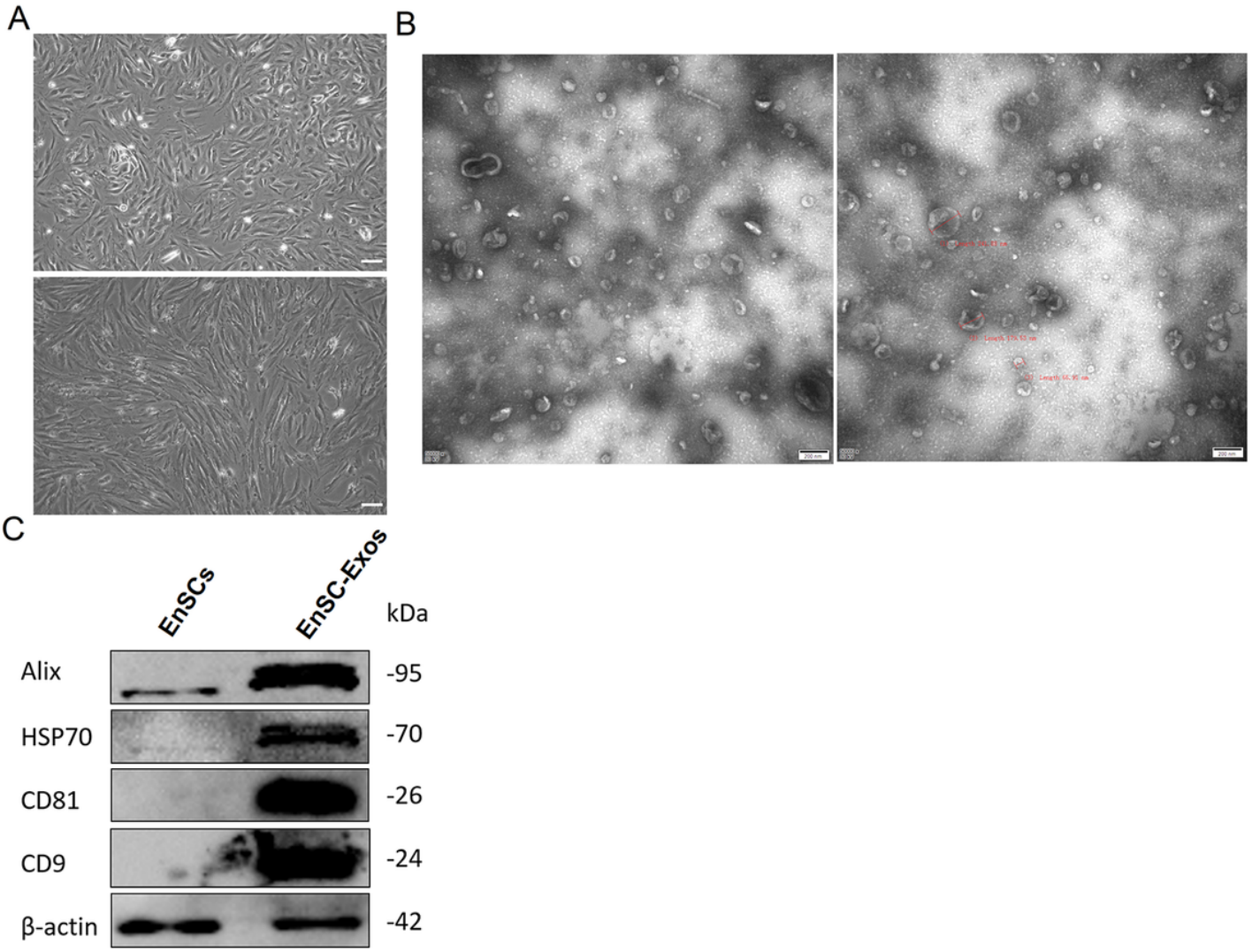

Figure 1

Isolation and identification of EnSC-Exos

(A) First (up panel) and third generation (down panel) EnSCs exhibited a typical fibroblastic morphology. Scale bar: 20 μm. (B) Exosomes isolated from human EnSCs conditioned medium were evidenced by electron microscopy. Scale bar: 200 nm. (C) Western blot analysis of Alix, HSP 70, CD81 and CD9 expression in EnSCs and EnSC-Exos. β-actin was used as a loading control.

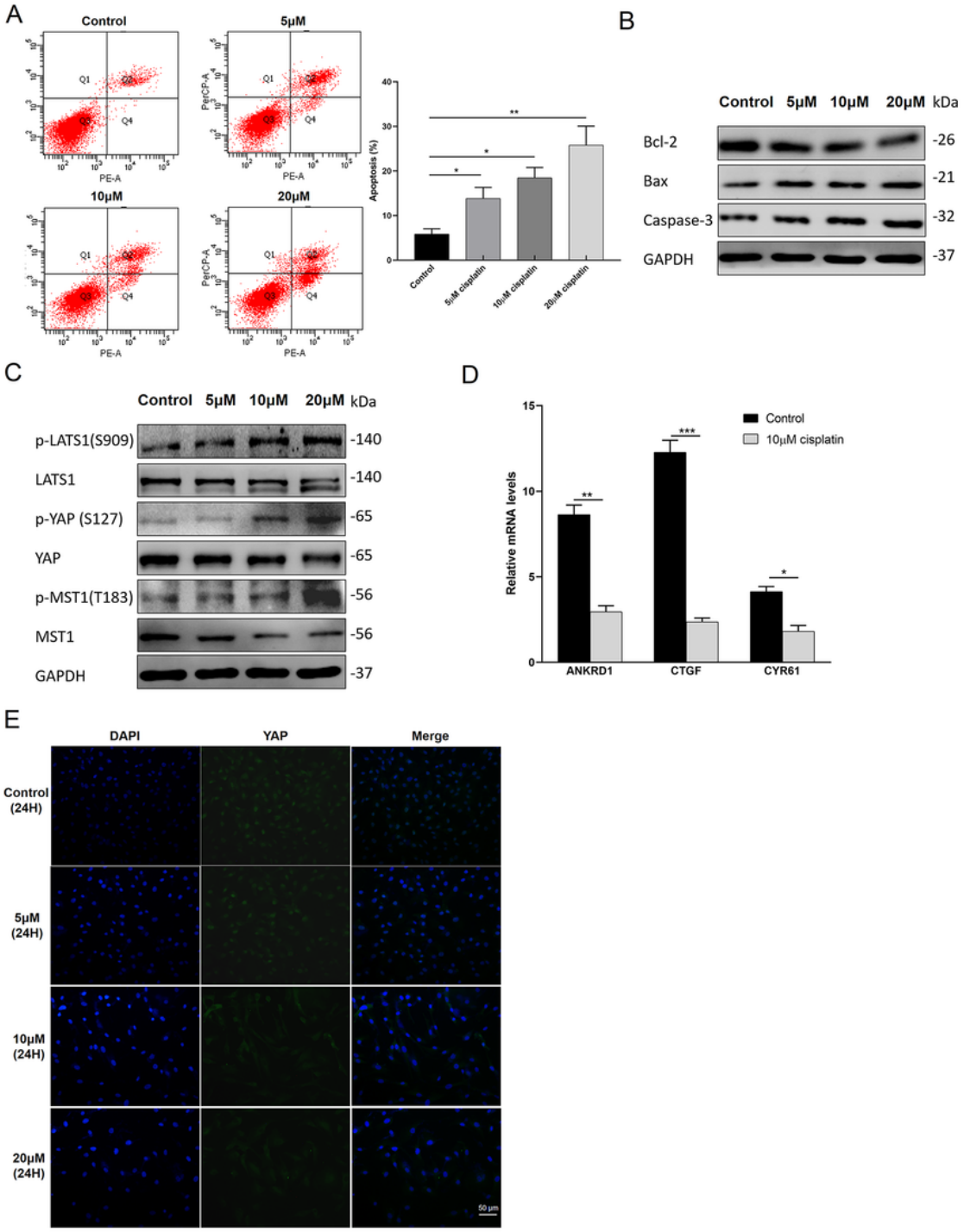

Figure 2

Cisplatin-damaged GCs induce the apoptosis *in vitro* through activating the Hippo signaling pathway

(A) Comparison of apoptotic rates of granulosa cells (GCs) between the groups by flow cytometry (left panel). Comparison of the percentages of apoptotic GCs in each group (right panel). Error bars represent SDs, $^{*}P < 0.05$, $^{**}P < 0.01$. (B) Western blot analysis of lysates with cisplatin-damaged GCs for 0, 5, 10 or

20 μM for 24 h with anti-Bcl-2, anti-Bax and anti-Caspase-3 antibodies. GAPDH was used as a loading control. (C) Cells were cultured in complete medium containing cisplatin (0, 5, 10, 20 μM) for 24 h. Western blot analysis of lysates from different groups with anti-p-LATS1, anti-LATS1, anti-p-YAP, anti-YAP, anti-p-MST anti-MST1 antibodies. GAPDH was used as a loading control. (D) Total RNA expression (qRT-PCR) of YAP target genes between Control group and Cisplatin group (cisplatin-damaged GCs for 10 μM for 24 h). Error bars represent SDs, $^{*}P < 0.05$, $^{**}P < 0.01$, $^{***}P < 0.001$. (E) Immunofluorescence staining indicating that expression of YAP is decreased in cisplatin-damaged GCs, compared to the Control group (YAP was stained with green, Nuclei were stained with blue). Scale bar: 50 μm.

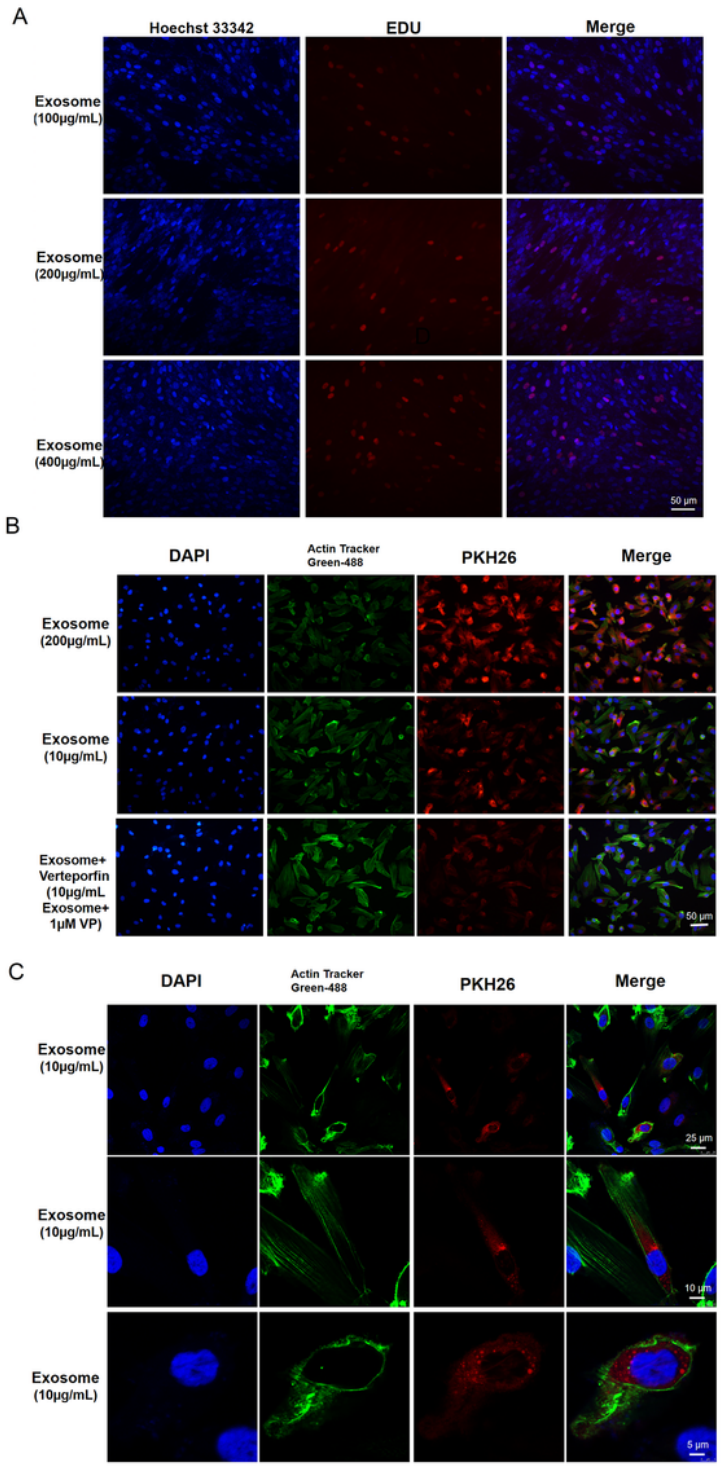

Figure 3

Uptake of EnSC-Exos by cisplatin-damaged GCs.

(A) Cell proliferation was determined by EdU labelling. EdU labelling analysis showed the fluorescence images of cisplatin-damaged GCs stimulated with 100, 200, 400 μg/mL EnSC-Exos and detected at 72 h after treatment (EdU, red fluorescent signals, DAPI, blue signals). Scale bar: 50 μm. (B) PKH26 labeled

exosomes were added along with or without Hippo inhibitor-Verteporfin and incubated at 37°C for 24 hours. Uptake of PKH26 labeled EnSC-Exos (red) in cisplatin-damaged GCs was evaluated with fluorescence microscopy. Cytoskeleton was stained with Actin-Tracker Green-488 (green). Nuclei were stained with DAPI (blue). Scale bar: 50 μm. (C) PKH26 labeled exosomes were added and incubated at 37°C for 24 hours. Uptake of 10 μg/mL PKH26-labeled EnSC-Exos (red) in cisplatin-damaged GCs was detected with confocal laser scanning microscope. Cytoskeleton was stained with Actin-Tracker Green-488 (green). Nuclei were stained with DAPI (blue).

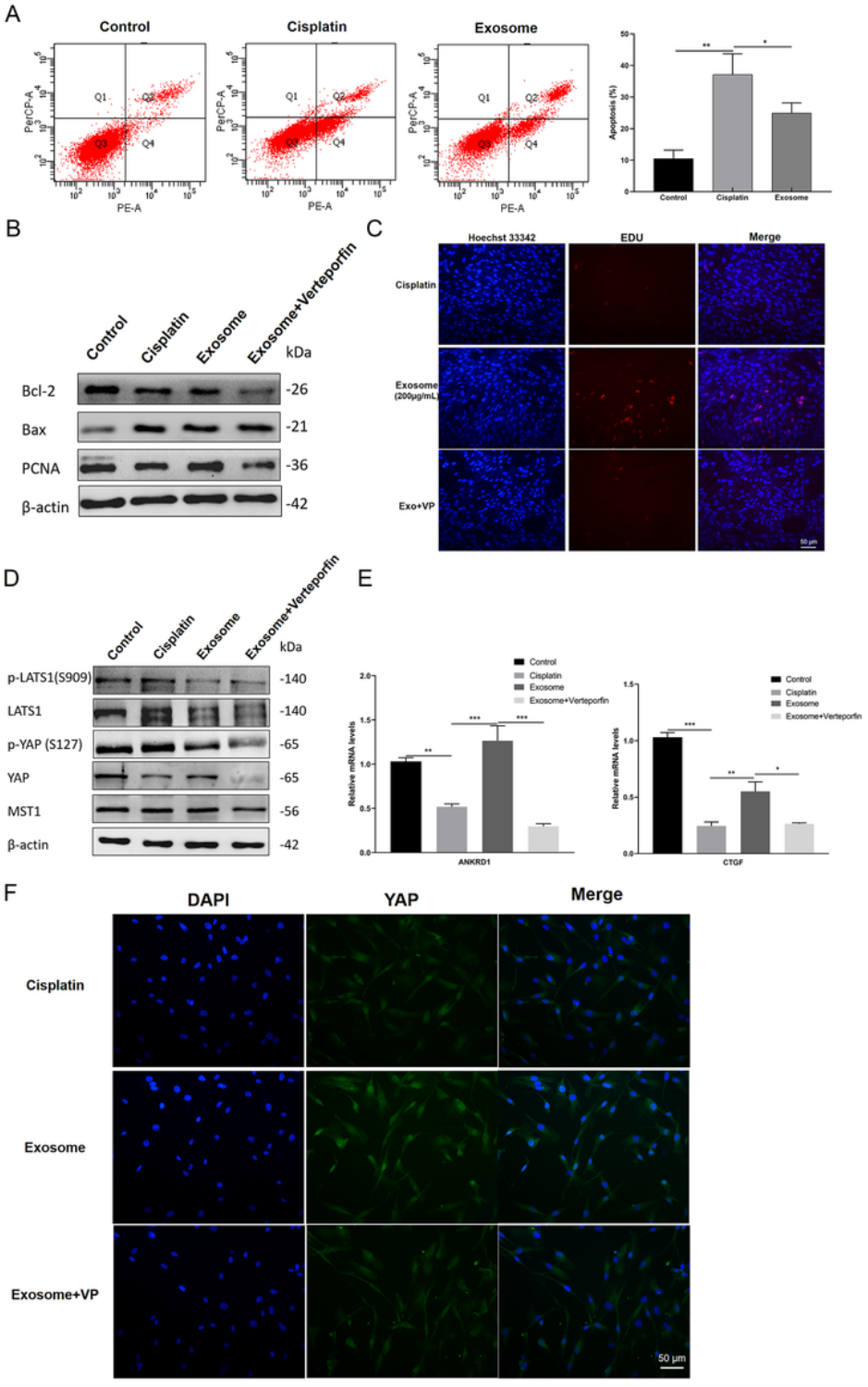

Figure 4

EnSC-Exos attenuated the apoptosis on cisplatin-damaged GCs by suppressing Hippo pathway *in vitro*

(A) The cell apoptosis assay was determined using flow cytometry analysis after the indicated treatment in different groups (left panel). Comparison of the percentages of apoptotic GCs in each group (right panel). Error bars represent SDs, $^{*}P < 0.05$, $^{**}P < 0.01$. (B) Western blot analysis of lysates compared with Control group, Cisplatin group, Exosome group and Exosome + Verteporfin group with anti-Bcl-2, anti-Bax and anti-PCNA antibodies. β-actin was used as a loading control. (C) Cell proliferation was determined by EdU labelling in different groups. EdU labelling analysis showed the fluorescence images of cisplatin-damaged GCs treatment with PBS (Cisplatin group), 200 μg/mL EnSC-Exos (Exosome group) and 200 μg/mL EnSC-Exos with 1 μM Verteporfin (Exosome + Verteporfin group) for 72 h (EdU, red fluorescent signals, DAPI, blue signals). Scale bar: 50 μm. (D) Western blot analysis of lysates from different groups with anti-p-LATS1, anti-LATS1, anti-p-YAP, anti-YAP and anti-MST1 antibodies. β-actin was used as a loading control. Cells were cultured in complete medium containing cisplatin (10 μM) for 24 h before treatment with PBS (Cisplatin group), 200 μg/mL EnSC-Exos (Exosome group) and 200 μg/mL EnSC-Exos with 1 μM Verteporfin (Exosome + Verteporfin group) for another 72 h. (E) Total RNA expression (qRT-PCR) of YAP target genes between different groups. Error bars represent SDs, $^{*}P < 0.05$, $^{**}P < 0.01$, $^{***}P < 0.001$. (F) Immunofluorescence staining indicating that exosomes caused YAP translocated into nucleus while Verteporfin significantly suppressed exosomes-induced YAP nuclear localization (YAP was stained with green, Nuclei were stained with blue). Scale bar: 50 μm.

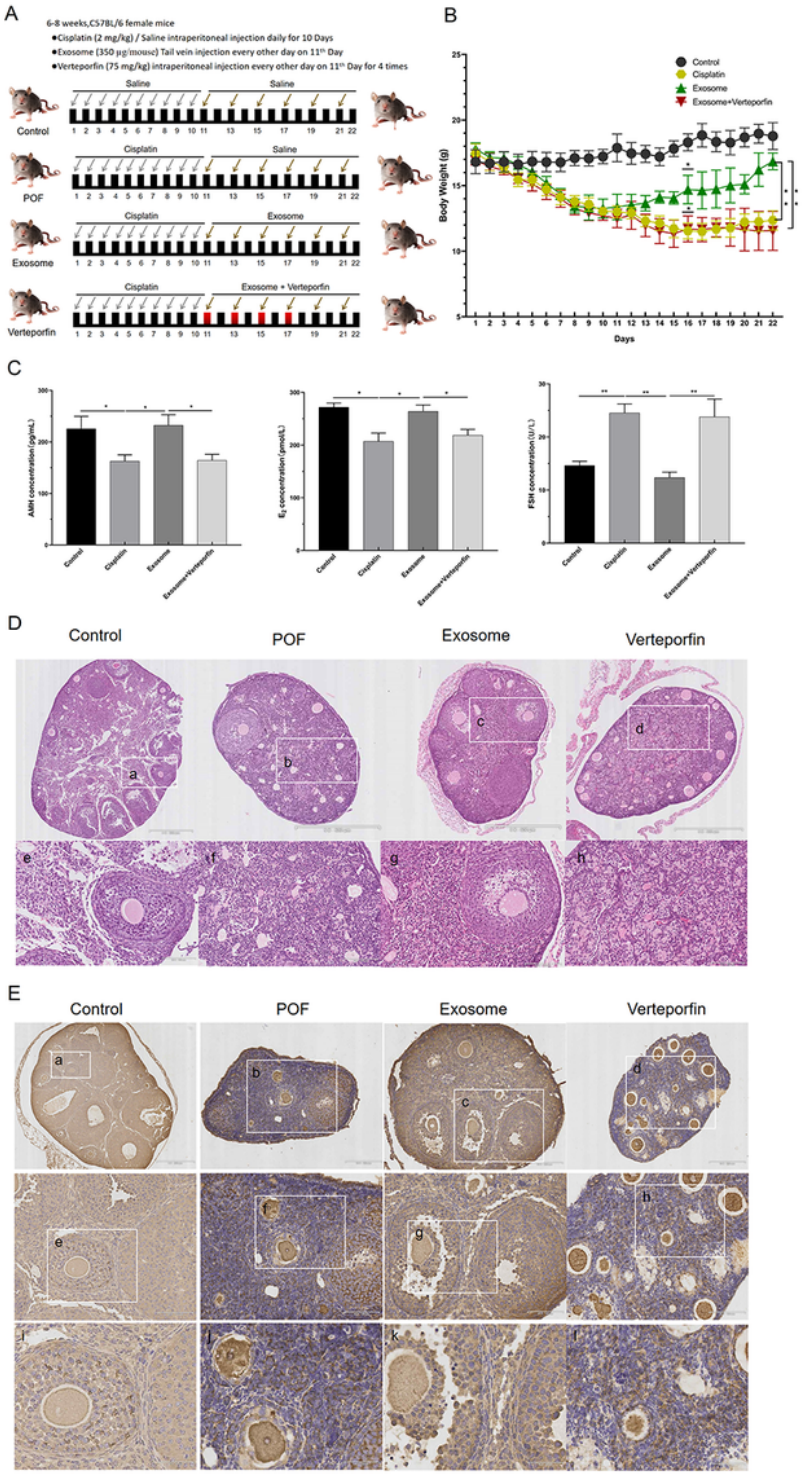

Figure 5

Diagram of the potential mechanisms involved in the effects of EnSC-Exos on cisplatin-induced GCs through Hippo pathway

(A) Schematic description of the experimental design. Cisplatin (2 mg/kg) was administered by intraperitoneal injection for 10 days. On day 11, human EnSC-Exos (350 μg/mouse) were transplanted by

tail vein injection. Verteporfin (75 mg/kg) intraperitoneal injection every other day on 10th Day for 4 times. Experimental analyses were performed after 3 weeks (22^{th}). (B) Body weight were measured each day in different groups. Error bars represent SDs, $^{*}P< 0.05$, $^{**}P< 0.01$. (C) The serum levels of AMH, E_2 and FSH in different groups. Data presented as mean ± SD. $^{*}P< 0.05$, $^{**}P< 0.01$. (D) Representative photomicrographs of H&E-stained ovarian sections in different groups. Scale bar = 4 × 500 μm (Control group) or 5 × 500 μm (POF, Exosome, Verteporfin group). Images e, f, g and h are magnifications of the squares in images a, b, c and d respectively. Scale bar = 20 × 100 μm (Control, POF, Exosome, Verteporfin group). (E) Representative photomicrographs of IHC analysis on YAP in ovarian tissue of mice in different groups. Photomicrographs show hematoxylin and DAB-stained ovaries. Brown in cytoplasm indicates positive expression of the YAP. Blue represents cell nuclear staining. Scale bar = 4 × 500 μm (Control group) or 10 × 200 μm (POF, Exosome, Verteporfin group), Images e, f, g and h are magnifications of the squares in images a, b, c and d respectively. Scale bar = 20 × 100 μm (Control, POF, Exosome, Verteporfin group), Images i, j, k and l are magnifications of the squares in images e, f, g and h respectively. Scale bar = 40 × 50 μm (Control, POF, Exosome, Verteporfin group).

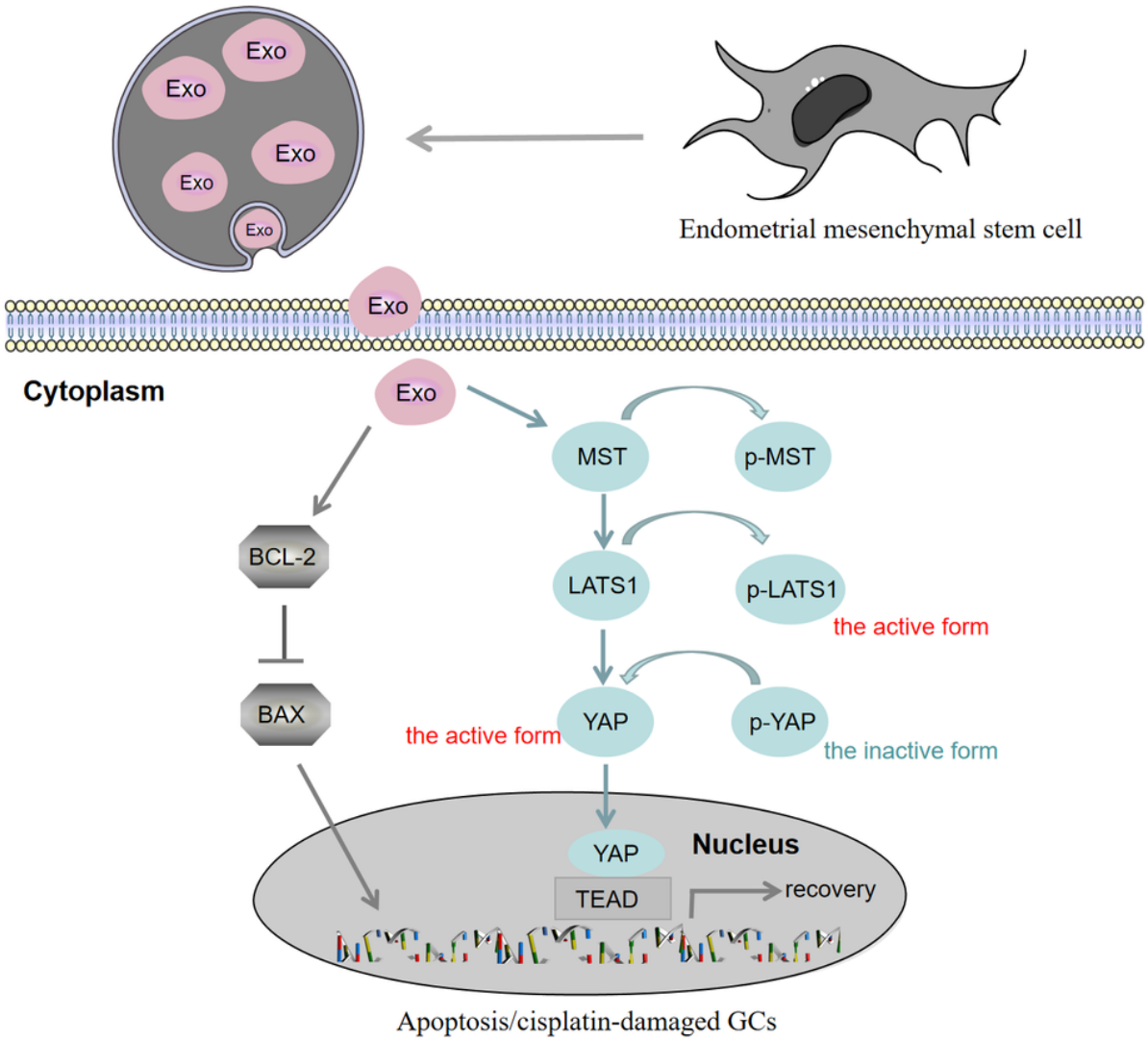

Figure 6

Diagram of the potential mechanisms involved in the effects of EnSC-Exos on cisplatin-induced GCs through Hippo pathway